JOURNAL OF SOLID STATE CHEMISTRY 93, 119–127 (1991)

Temperature-Dependent Structure and Anisotropic Debye–Waller Factors of the Dimer Compound $Cs_3Ho_2Br_9$

A. DÖNNI, P. FISCHER, AND A. FURRER

Laboratory for Neutron Scattering, ETH, Zürich, CH-5232 Villigen PSI, Switzerland

J. K. COCKCROFT

Institut Laue-Langevin, F-38042 Grenoble, France

AND H. U. GÜDEL

Institute for Inorganic Chemistry, University, Freiestr. 3, CH-3000 Bern 9, Switzerland

Received November 14, 1990; in revised form February 28, 1991

The temperature-dependent structure of the dimer compound $Cs_3Ho_2Br_9$ was investigated in great detail with use of the high-resolution neutron powder diffractometer D2B at ILL (Grenoble). The refinement of around 2350 nuclear reflections within the trigonal space group $R\bar{3}c$ yields largely anisotropic thermal vibrations of the Br atoms in contrast to Cs and Ho. The orientations of the thermal ellipsoids are reasonable when considering the reduced distances within the dimeric units $Ho_2Br_9^{3-}$. Additional low temperature neutron diffraction experiments performed down to $T = 7$ mK did not give evidence for long-range magnetic ordering.

Introduction

Rare earth compounds of composition $Cs_3R_2Br_9$ (R = Lu, Yb, Tm, Er, Ho, Dy, Tb, Gd, Sm) are known to crystallize in the trigonal space group $R\bar{3}c$ with $Z = 6$ (*1*, *2*), in the so-called $Cs_3Tl_2Cl_9$ structure (*3*). The structure contains the dimeric units $R_2Br_9^{3-}$, which are built up of two face-sharing RBr_6^{3-} octahedra as illustrated in Fig. 1.

We have shown that the study of dimer systems by inelastic neutron scattering provides a very direct way to establish exchange splittings and thus exchange parameters (*5–7*). First results of these studies performed for several compounds $Cs_3R_2Br_9$ show that for R = Tb, Dy, Yb a Heisenberg model adequately describes the observed splittings as long as only one crystal-field state is considered (*5*, *6*). For R = Ho it was found that for a proper reproduction of the observed splittings in three crystal-field states an (anisotropic) exchange-tensor formalism was most appropriate (*7*). So far we have not yet attempted to quantitatively discuss our results; however, it is clear that a detailed understanding of exchange parameters requires a detailed knowledge of the structural parameters, since both dipole–di-

0022-4596/91 $3.00

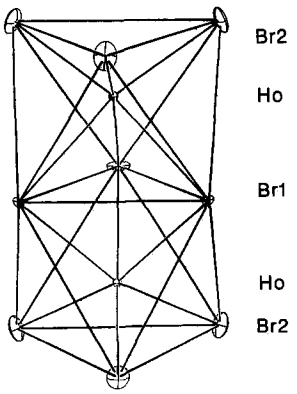

FIG. 1. ORTEP plot (*4*) of the dimeric unit $Ho_2Br_9^{3-}$ showing the anisotropic thermal ellipsoids at T = 150 K.

pole and superexchange interactions depend on interatomic distances and superexchange pathways through the ligand ions, respectively.

Previous powder neutron diffraction experiments have been performed at T = 8 K and at room temperature to study the influence of different rare-earth elements to the trigonal structure of the $Cs_3R_2Br_9$ compounds (*2*). The lanthanide contraction results in a decrease of the lattice constants with increasing atomic number, which is more pronounced for a than for c.

In the present study the temperature-dependent structure of the dimer compound $Cs_3Ho_2Br_9$ has been investigated by neutron diffraction from 1.5 K to room temperature in great detail. The temperature dependence of the structure will be very helpful in understanding a possible variation of the exchange parameters with temperature, which for some transition metal dimers turned out to be rather large, typically 10% between zero and room temperature (*8*). In addition, we have performed experiments at very low temperature (T = 7 mK) in order to search for possible long-range magnetic ordering.

Experimental

The polycrystalline compound $Cs_3Ho_2Br_9$ was synthesized as described in the literature (*9*). The sample was enclosed under helium atmosphere into a cylindrical vanadium container of 10 mm diameter and 50 mm height. Measurements in the temperature range from 1.5 to 295 K were performed at the Institut Laue-Langevin (ILL), Grenoble, with use of the high-resolution neutron powder diffractometer D2B operated in the high-intensity mode and using a scattering angle step width of 0.05°. The temperatures were achieved using an ILL standard ^{4}He cryostat. The incident neutron wavelengths λ = 1.277 Å and λ = 1.594 Å were obtained from Ge (3, 3, 7) and Ge (3, 3, 5) monochromators, respectively.

In order to search for magnetic ordering the sample was filled into a cylindrical copper container of 8 mm diameter and was cooled down to 7 mK using a ^{3}He/^{4}He dilution refrigerator cryostat. This study was performed at the reactor Saphir, Würenlingen, with use of the diffractometer DMC (*10*) with λ = 1.704 Å operated in the high-intensity mode. Cryostat peaks were suppressed by an oscillating radial collimator.

Results

The D2B diffraction patterns were analyzed with a modified version of the program of Wiles and Young (*11*), including a fit of the background represented by a self-adjusting polynomial. The refinement is based on the following neutron scattering lengths (10^{-12} cm): Cs, 0.542; Br, 0.679; and Ho, 0.808 (*12*). Absorption corrections were neglected since the expected corrections for the Debye–Waller factors ΔB = −0.03 Å^2 (for λ = 1.594 Å and μR = 0.205) and ΔB = −0.01 Å^2 (for λ = 1.277 Å and μR = 0.164) are within the errors of the fit (*13*). The use of a pseudo-Voigt peak shape produced a slightly better quality of the fits

TABLE 1

STRUCTURAL PARAMETERS AND ISOTROPIC DEBYE–WALLER FACTORS OF $Cs_3Ho_2Br_9$ OBTAINED FROM A WILES AND YOUNG REFINEMENT OF D2B NEUTRON POWDER DATA MEASURED WITH $\lambda = 1.594$ Å

T (K)	a (Å)	c (Å)	c/a	Cs: x/a	Cs: B (Å^2)
1.5	13.4685 (2)	19.0879 (3)	1.41723 (5)	0.6615 (4)	0.39 (6)
25	13.4705 (2)	19.0924 (4)	1.41735 (5)	0.6614 (4)	0.52 (7)
50	13.4789 (2)	19.1091 (4)	1.41770 (6)	0.6616 (4)	0.65 (7)
75	13.4894 (2)	19.1298 (4)	1.41813 (6)	0.6612 (4)	0.86 (8)
100	13.5009 (3)	19.1519 (4)	1.41856 (6)	0.6609 (4)	1.01 (8)
150	13.5256 (3)	19.1989 (5)	1.41945 (7)	0.6610 (5)	1.55 (9)
200	13.5512 (3)	19.2500 (6)	1.42054 (8)	0.6610 (6)	2.0 (1)
260	13.5814 (4)	19.3126 (7)	1.4220 (1)	0.6607 (7)	2.7 (1)
295	13.6022 (5)	19.3571 (8)	1.4231 (1)	0.6605 (8)	3.1 (2)

T (K)	Ho: z/c	Ho: B (Å^2)	Br1: x/a	Br1: B (Å^2)	Br2: x/a
1.5	0.6498 (1)	0.07 (4)	0.1586 (2)	0.40 (5)	0.1800 (1)
25	0.6497 (1)	0.07 (4)	0.1587 (2)	0.43 (5)	0.1798 (2)
50	0.6499 (1)	0.14 (4)	0.1585 (3)	0.57 (6)	0.1798 (2)
75	0.6498 (1)	0.25 (4)	0.1583 (3)	0.67 (6)	0.1794 (2)
100	0.6499 (2)	0.38 (5)	0.1581 (3)	0.76 (6)	0.1792 (2)
150	0.6499 (2)	0.54 (5)	0.1582 (3)	1.02 (7)	0.1789 (2)
200	0.6498 (2)	0.74 (6)	0.1578 (4)	1.43 (9)	0.1784 (2)
260	0.6499 (2)	0.99 (7)	0.1576 (4)	1.7 (1)	0.1778 (3)
295	0.6500 (2)	1.17 (7)	0.1577 (4)	1.9 (1)	0.1778 (3)

T (K)	Br2: y/a	Br2: z/c	Br2: B (Å^2)	R_w (%)	R_e (%)	χ^2	R_I (%)
1.5	0.1740 (2)	0.0850 (1)	0.35 (3)	11.5	5.7	4.0	4.4
25	0.1739 (2)	0.0852 (1)	0.41 (3)	11.8	5.8	4.1	4.6
50	0.1738 (2)	0.0853 (2)	0.59 (4)	12.1	6.0	4.1	5.1
75	0.1736 (2)	0.0855 (2)	0.80 (4)	12.4	6.3	3.9	5.4
100	0.1732 (2)	0.0858 (2)	0.96 (4)	12.7	6.5	3.8	5.8
150	0.1729 (3)	0.0862 (2)	1.38 (5)	13.6	7.0	3.8	7.0
200	0.1723 (3)	0.0861 (2)	1.80 (6)	14.4	7.6	3.6	8.1
260	0.1719 (4)	0.0863 (2)	2.38 (7)	15.6	8.1	3.7	9.3
295	0.1708 (4)	0.0866 (3)	2.74 (8)	16.2	8.5	3.6	10.4

Note. Trigonal space group $R\bar{3}c$ with Cs (18*e*): x/a, 0, $\frac{1}{4}$; Ho (12*c*): 0, 0, z/c; Br1 (18*e*): x/a, 0, $\frac{1}{4}$; Br2 (36*f*): x/a, y/a, z/c.

compared to a Gaussian peak shape (e.g., for $\lambda = 1.594$ Å and $T = 1.5$ K we obtained $\chi^2 = 4.0$ for pseudo-Voigt and $\chi^2 = 4.4$ for Gaussian peak shape).

About 1200 nuclear (*hkl*) values in the range $9° \leq 2\Theta \leq 154°$ were refined from 2901 data points (step $\Delta 2\Theta = 0.05°$, no excluded regions) in the spectra obtained with $\lambda = 1.594$ Å at nine different temperatures. Structural parameters and isotropic Debye–Waller factors are listed in Table I. The conventional agreement values such as expected from counting statistics (R_e), weighted profile (R_w), and integrated Bragg intensities (R_I) are defined in Ref. (*14*). The relative errors given in parentheses include estimated standard deviations of the fit. From the uncertainty of the neutron wavelength $\lambda = (1.594 \pm 0.001)$ Å the absolute errors amount to $a = 13.602(9)$ Å and $c =$

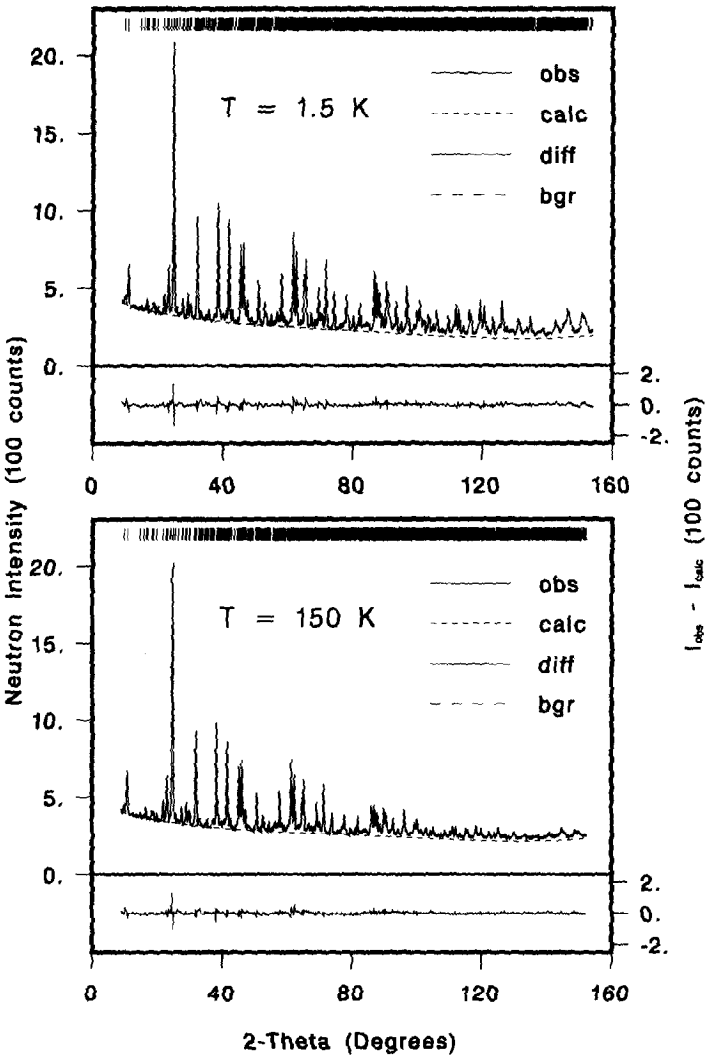

FIG. 2. Observed (obs), calculated (calc) including background (bgr) and difference (diff) neutron diffraction patterns of $Cs_3Ho_2Br_9$ at T = 1.5 and 150 K, measured with λ = 1.277 Å.

19.36(1) Å for the room temperature lattice parameters, whereas the structural parameters x/a, y/a, and z/c are not affected.

The spectra obtained with λ = 1.277 Å at 1.5 and 150 K are shown in Fig. 2, where the paramagnetic contribution to the background (decreasing intensity with increasing 2Θ value) can be nicely seen. About 2350 nuclear (hkl) values were refined in the range $9° \leq 2\Theta \leq 154°$ for $T \approx 1.5$ K and $9° \leq 2\Theta \leq 152°$ for T = 150 K, with no excluded regions and the step $\Delta 2\Theta$ = 0.05° corresponding to 2901 and 2861 data points at 1.5 and 150 K, respectively. The resulting structural parameters and isotropic Debye–Waller factors are listed in Table II. Again relative errors are given in parentheses.

TABLE II

STRUCTURAL PARAMETERS AND ISOTROPIC DEBYE–WALLER FACTORS OF $Cs_3Ho_2Br_9$ OBTAINED FROM A WILES AND YOUNG REFINEMENT OF D2B NEUTRON POWDER DATA MEASURED WITH λ = 1.277 Å

$Cs_3Ho_2Br_9$	T = 1.5 K	T = 150 K
a (Å)	13.4700 (2)	13.5244 (4)
c (Å)	19.0894 (4)	19.1987 (7)
c/a	1.41718 (5)	1.41956 (9)
Cs		
x/a	0.6621 (3)	0.6618 (5)
B (Å^2)	0.36 (5)	1.36 (9)
Ho		
z/c	0.6500 (1)	0.6499 (1)
B (Å^2)	0.00 (3)	0.22 (5)
Br1		
x/a	0.1588 (2)	0.1586 (3)
B (Å^2)	0.14 (4)	0.70 (6)
Br2		
x/a	0.1802 (1)	0.1790 (2)
y/a	0.1743 (2)	0.1736 (3)
z/c	0.0846 (1)	0.0858 (2)
B (Å^2)	0.36 (3)	1.50 (5)
R_w (%)	10.5	12.6
R_e (%)	3.7	5.7
χ^2	7.9	5.0
R_I (%)	5.4	8.3

Note. Trigonal space group $R\bar{3}c$ with Cs (18*e*): x/a, 0, ¼; Ho (12*c*): 0, 0, z/c; Br1 (18*e*): x/a, 0, ¼; Br2 (36*f*): x/a, y/a, z/c.

In addition anisotropic Debye–Waller factors B_{ij} were refined in the spectra with T = 150 K and λ = 1.277 Å. The results of the fit together with the calculated components along the principal axes (B_1, B_2, and B_3) of the thermal ellipsoids are listed in Table III. Due to symmetry constraints (*15*) the number of independent Debye–Waller factors is reduced from 6 to 2 and to 4 for the atomic positions (12*c*) and (18*e*), respectively. For sites (12*c*) the directions of the principal axes are restricted by symmetry to be parallel to the c axis (B_3) and to be isotropic in the ab plane ($B_2 = B_1$). Due to the symmetry constraints for Cs and Br1 on position (x/a, 0, ¼) of sites (18*e*) one principal axis (B_1) has to be parallel to the a direction. As a result of the fit (see Table III) for both atoms Cs and Br1 the thermal parameters B_{13} and B_{23} vanish within the experimental errors; thus the principal axis B_3 turns out to be parallel to the c axis. B_2 is left to be perpendicular to both the c axis and the a axis. For Br2 on general positions (36*f*) all B_{ij} values are independent. Within the experimental errors the following directions of the principal axes were determined from Table III: B_3 points toward the intradimeric nearest neighbor Ho atom, and B_2 is perpendicular to both the B_3 direction and the c axis.

The experiment with the dilution cryostat proves paramagnetism of $Cs_3Ho_2Br_9$ between 7 mK and room temperature. No magnetic Bragg peaks were observed in the difference spectra 1.2 K–7 mK.

Discussion

The room-temperature lattice constants of $Cs_3Ho_2Br_9$ are in excellent agreement

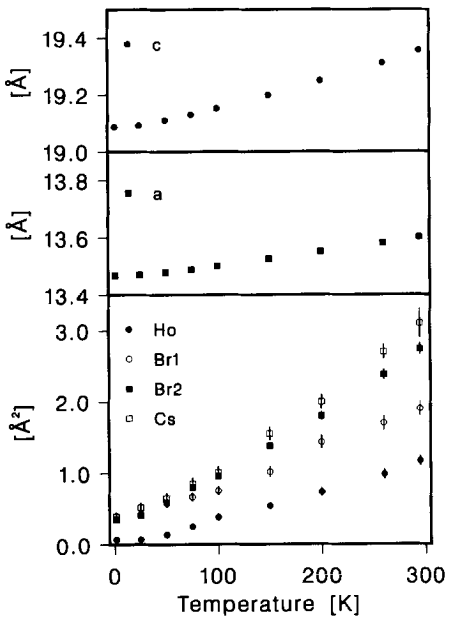

FIG. 3. Temperature dependence of lattice constants a, c and isotropic Debye–Waller factors of $Cs_3Ho_2Br_9$.

TABLE III

ANISOTROPIC DEBYE–WALLER FACTORS B_{ij} AND THE COMPONENTS ALONG PRINCIPAL AXES (B_1, B_2, B_3) OF THE THERMAL VIBRATION ELLIPSOIDS OF $Cs_3Ho_2Br_9$ AT 150 K MEASURED WITH λ = 1.277 Å

$Cs_3Ho_2Br_9$		T = 150 K		Space group $R\bar{3}c$
a = 13.5424 (4) Å		c = 19.1984 (7) Å		c/a = 1.4195 (1)
	x/a	y/a		z/c
(18*e*) Cs	0.6612 (5)	0		0.25
(12*c*) Ho	0	0		0.6501 (1)
(18*e*) Br1	0.1581 (1)	0		0.25
(36*f*) Br2	0.1792 (2)	0.1737 (3)		0.0849 (2)

	B_{11} (Å^2)	B_{22} (Å^2)	B_{33} (Å^2)	B_{12} (Å^2)	B_{13} (Å^2)	B_{23} (Å^2)
(18*e*) Cs	1.1 (2)	1.4 (2)	1.5 (2)	0.7	0.0 (2)	0.0
(12*c*) Ho	0.34 (9)	0.34	0.1 (1)	0.17	0	0
(18*e*) Br1	0.5 (2)	2.2 (2)	0.3 (2)	1.1	0.0 (2)	0.0
(36*f*) Br2	0.7 (1)	0.9 (1)	2.2 (1)	0.00 (8)	0.6 (1)	0.5 (1)

R_w = 11.9%	R_e = 5.6%	χ^2 = 4.5	R_I = 7.0%
	B_1 (Å^2)	B_2 (Å^2)	B_3 (Å^2)
(18*e*) Cs	1.0 (1)	1.4 (2)	1.5 (2)
(12*c*) Ho	0.34 (9)	0.34 (9)	0.1 (1)
(18*e*) Br1	0.0 (1)	2.2 (2)	0.3 (2)
(36*f*) Br2	2.5 (1)	1.6 (2)	0.3 (1)

Note. For symmetry constraints see Ref. (*15*). Directions of the principal axes are explained in the text.

with the X-ray values a = 13.603 Å and c = 19.36 Å (*a*). Lattice constants a, c and isotropic Debye–Waller factors as a function of temperature are illustrated in Fig. 3. As shown in Table I the value c/a increases with increasing temperature, confirming the anisotropic thermal expansion of the lattice constants reported in Ref. (*2*).

Previous neutron diffraction experiments (*2*) performed at T = 8 K and T = 295 K in a limited 2Θ range indicated an increase of the molecular character of the dimeric units $Ho_2Br_9^{3-}$ with increasing temperature. This result is confirmed by the present high-resolution neutron diffraction study with more accurate structural parameters and a more detailed temperature dependence. Selected intradimeric and interdimeric distances are listed in Table IV and illustrated in Fig. 4.

The dimeric units $Ho_2Br_9^{3-}$ shown in Fig. 1 are of particular interest. Heating $Cs_3Ho_2Br_9$ from 1.5 K to room temperature causes an increase in the interdimeric terminal Br2–Br2 distance (2×) and the Cs–Br mean distance (12×) by 2.0 (4)% and 1.3 (3)%, respectively. The dimer units $Ho_2Br_9^{3-}$ become increasingly isolated both from each other and from the Cs^+ ions. The change of intradimeric distances is smaller and either positive for Ho–Br1: +0.7 (2)%, zero within the error of the fit in the case of Br1–Br1: +0.4 (4)%, or negative for Ho–Br2: −0.6 (3)% and for Br2–Br2: −0.5 (2)%. The increase of the intradimeric distance Ho–Ho of +1.3 (4)% reflects the thermal expansion of the lattice constant c, since the atomic position of Ho (12*c*); (0, 0, z/c) in relative units z/c = 0.650 is temperature

TABLE IV

TEMPERATURE DEPENDENCE OF SELECTED INTRADIMERIC AND INTERDIMERIC DISTANCES OF $Cs_3Ho_2Br_9$ IN Å

T(K)	Ho–Ho (1×)[a]	Ho–Br1 (3×)[a]	Ho–Br2 (3×)[a]	Br1–Br1 (2×)[a]
1.5	3.825 (4)	2.867 (3)	2.687 (2)	3.700 (5)
25	3.830 (4)	2.870 (3)	2.683 (3)	3.703 (5)
50	3.826 (4)	2.868 (4)	2.685 (3)	3.700 (7)
75	3.834 (4)	2.870 (4)	2.681 (3)	3.699 (7)
100	3.834 (8)	2.869 (4)	2.678 (3)	3.697 (7)
150	3.844 (8)	2.876 (4)	2.676 (4)	3.706 (7)
200	3.858 (8)	2.880 (5)	2.675 (4)	3.704 (10)
260	3.866 (8)	2.884 (5)	2.675 (4)	3.707 (10)
295	3.872 (8)	2.889 (5)	2.671 (5)	3.715 (10)
T (K)	Br2–Br2 (3×)[a]	Br2–Br2 (2×)[b]	Cs–Br2 (12×)[c]	
1.5	4.131 (3)	4.027 (4)	3.877 (4)	
25	4.128 (4)	4.033 (4)	3.878 (4)	
50	4.129 (4)	4.039 (7)	3.881 (4)	
75	4.126 (4)	4.047 (7)	3.886 (5)	
100	4.122 (4)	4.058 (7)	3.890 (5)	
150	4.123 (5)	4.077 (7)	3.899 (5)	
200	4.118 (5)	4.079 (7)	3.909 (6)	
260	4.115 (6)	4.093 (7)	3.921 (7)	
295	4.109 (6)	4.107 (10)	3.929 (8)	

[a] Intradimeric distance.
[b] Interdimeric terminal Br2–Br2 distance.
[c] Mean distance Cs–Br.

independent (cf. Table I). Thus the increasing separation of the dimeric units $Ho_2Br_9^{3-}$ along the c direction is due to an increasing intradimeric attraction of the negative terminal Br2 ions by the positive Ho^{3+} ions with increasing temperature.

The intradimeric Ho–Br2 distance (Fig. 4) is typically 0.2 Å smaller than the Ho–Br1 distance, which is roughly equal to the sum of the respective ionic radii (*2*). The bridging Br1 ions are shielding the electrostatic repulsion of the two intradimeric Ho^{3+} ions. This causes the Br1–Br1 distance to be reduced by about 0.4 Å compared to the intradimeric terminal Br2–Br2 distance, which is also roughly equal to the sum of the respective ionic radii. The reduction of intradimeric distances Ho–Br2 and Br1–Br1 is similar to that observed in $Cs_3Tb_2Br_9$ and $Cs_3Er_2Br_9$ and can be rationalized by simple electrostatic arguments as described in Ref. (*2*).

The anisotropic thermal ellipsoids within the dimeric unit $Ho_2Br_9^{3-}$ at T = 150 K are plotted in Fig. 1. The thermal vibrations of the negative ions Br1 and Br2 show large anisotropies in contrast to the positive ions Cs^+ and Ho^{3+} (see results in Table III). The shapes of the anisotropic thermal ellipsoids of Br1 and Br2 are reasonable when looking at the intradimeric distances. The principal axes of the Br2 ellipsoid consist of two large and one small component, the latter being parallel to the reduced Ho–Br2 distance. There are one large and two small components along the principal axes of the Br1 ellipsoid. The smallest component (zero within the error of the fit) directs to the cen-

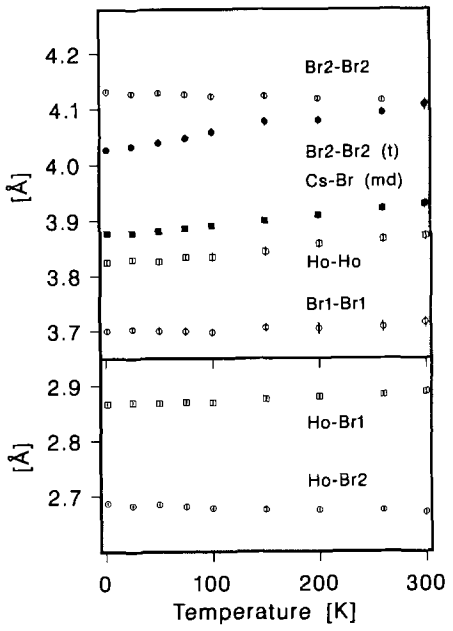

FIG. 4. Temperature dependence of selected interatomic distances in $Cs_3Ho_2Br_9$. Intradimeric distances: Ho–Ho, Ho–Br1, Ho–Br2, Br1–Br1, Br2–Br2; interdimeric terminal Br2–Br2 distance: Br2–Br2 (t) and Cs–Br mean distance: Cs–Br (md).

ter of the triangle formed by the three Br1 atoms, which have largely reduced Br1–Br1 distances. The other small component is parallel to the c direction, the Ho^{3+}–Ho^{3+} axis.

The refined isotropic Debye–Waller factors of Ho and Br1 (Table I) show a strongly correlated temperature dependence, as can be seen in Fig. 3. The generally large obtained values for isotropic Debye–Waller factors at higher temperatures are proven by the remarkable decrease of observed coherent neutron intensity at large 2Θ values (see Fig. 2).

Conclusion

The absence of long-range magnetic ordering in $Cs_3Ho_2Br_9$ at $T = 7$ mK is surprising. Although the electronic ground state is a (nonmagnetic) singlet, there is a low-lying doublet about 70 μeV above the ground state (*7*). Thus we have anticipated that the interdimer interaction is able to sufficiently admix an induced moment to the singlet ground-state and thereby to realize long-range magnetic ordering. In fact, in the isostructural compound $Cs_3Er_2Br_9$ long-range antiferromagnetic ordering was observed below 1.2 K (*16*). In singlet ground-state systems the condition for the occurrence of long-range magnetic ordering is given (*17*) by

$$\frac{4 \cdot J(0) \cdot \alpha^2}{\Delta} \geq 1,$$

where $J(0)$ is the molecular-field parameter and α the matrix element for dipole transitions between the singlet ground state and the next higher level energetically separated by Δ. With $\Delta = 70$ μeV and $\alpha^2 = 1.6$ (*7*) we conclude that the interdimer coupling parameter in $Cs_3Ho_2Br_9$ is below the critical value $J(0) \approx 10^{-2}$ meV.

With respect to the intradimeric exchange coupling the temperature dependence of the intradimer Ho–Ho distance, which increases by as much as 0.05 Å when the temperature is raised from 1.5 K to 295 K, is particularly intriguing (see Table IV), e.g., magnetostriction effects derived for the antiferromagnet $CsMnBr_3$ (*18*) resulted in a 15% change of the nearest-neighbor exchange parameter when the corresponding bond length is compressed or expanded by 0.01 Å. Therefore it would be interesting to measure the temperature dependence of the intradimer exchange coupling in $Cs_3Ho_2Br_9$, since magnetostriction effects are expected to be even larger for f-electrons than for d-electrons.

Acknowledgments

We are indebted to N. Furer for preparing the sample and to J. Davies and S. Fischer for the expert technical assistance in the experiments. Financial support by

the Swiss National Science Foundation is gratefully acknowledged.

References

1. G. MEYER AND A. SCHÖNEMUND, *Mater. Res. Bull.* **15,** 89 (1980).
2. A. DÖNNI, A. FURRER, AND H. U. GÜDEL, *J. Solid State Chem.* **81,** 278 (1989).
3. J. L. HOARD AND L. GOLDSTEIN, *J. Chem. Phys.* **3,** 199 (1935).
4. G. DAVENPORT, S. HALL, AND W. DREISSIG, "ORTEP" XTAL2.6 User's Manual (S. R. Hall and J. M. Stewart, Eds.), Universities of Western Australia and Maryland.
5. A. DÖNNI, A. FURRER, H. BLANK, A. HEIDE MANN, AND H. U. GÜDEL, *J. Phys. Colloq.* **49,** C8–1513 (1988).
6. A. FURRER, H. U. GÜDEL, H. BLANK, AND A. HEIDEMANN, *Phys. Rev. Lett.* **62,** 210 (1989).
7. A. FURRER, H. U. GÜDEL, E. R. KRAUSZ, AND H. BLANK, *Phys. Rev. Lett.* **64,** 68 (1990).
8. H. U. GÜDEL, A. FURRER, W. BÜHRER, AND B. HÄLG, *Surf. Sci.* **106,** 432 (1981).
9. G. MEYER, *Inorg. Synth.* **22,** 1 (1983).
10. J. SCHEFER, P. FISCHER, H. HEER, A. ISACSON, M. KOCH, AND R. THUT, *Nucl. Instr. Methods Phys. Res. Sect. A* **288,** 477 (1990).
11. D. B. WILES AND R. A. YOUNG, *J. Appl. Crystallogr.* **15,** 430 (1982).
12. V. F. SEARS, "Methods of Experimental Physics," Vol. 23A, Academic Press, Orlando, FL (1986).
13. A. W. HEWAT, *Acta Crystallogr. Sect. A* **35,** 248 (1979).
14. G. MALMROS AND J. O. THOMAS, *J. Appl. Crystallogr.* **10,** 7 (1977).
15. W. J. A. M. PETERSE AND J. H. PALM, *Acta Crystallogr.* **20,** 147 (1966).
16. A. DÖNNI, P. FISCHER, AND A. FURRER, Report LNS 150, ETH Zürich, p. 55, unpublished (1990).
17. B. R. COOPER, "Magnetic Properties of Rare Earth Metals" (R. J. Elliott, Ed.), p. 17. Plenum, London (1972).
18. U. FALK, A. FURRER, J. K. KJEMS, AND H. U. GÜDEL, *Phys. Rev. Lett.* **52,** 1336 (1984).